Article

Dynamic Testing in Support of the Seismic Assessment of a Century Old Masonry Building Complex

Michele Dilena [ID], Marta Fedele Dell'Oste, Alessandra Gubana [ID], Antonino Morassi [ID] and Eric Puntel *[ID]

Polytechnic Department of Engineering and Architecture, University of Udine, Via delle Scienze 206, 33100 Udine, Italy; michele.dilena@uniud.it (M.D.); martafedele@hotmail.com (M.F.D.); alessandra.gubana@uniud.it (A.G.); antonino.morassi@uniud.it (A.M.)
* Correspondence: eric.puntel@uniud.it; Tel.: +39-0432-558735

Abstract: The vulnerability assessment of existing masonry buildings is a largely investigated research topic with some aspects still to be faced. In historic towns, masonry buildings are aggregated and together confined, and their final appearance is derived from interventions and additions during their lives in different times and with different masonry textures or different construction materials. Demolitions and reconstructions of some parts were frequent, with the difficulty of now understanding the effectiveness of the mutual constraints. The seismic assessment of a case study of a 175-year-old building complex in Udine (Italy) provides an opportunity to use the results of ambient vibration tests to face the problem of modelling aggregate buildings for their seismic assessment. The "Padiglione Lodi" building complex was built in 1847 and extended and renovated several times afterwards. It was built mostly using URM with limited use of reinforced concrete. It consists of a main building and three wings (western, central and eastern). The inspections, experimental survey and analysis of the available documentation are used to suitably calibrate a Finite Element Model of the whole complex. Moreover, this allows the singling out of the central wing, as the unit needs more careful investigation. Non-destructive dynamic testing is then applied to the central wing in order to further validate the model and improve the knowledge of the interaction of the unit with the rest of the building. General remarks on the effective application of non-destructive dynamic analysis in conjunction with other methods to the seismic assessment of large URM building complexes are drawn.

Keywords: un-reinforced masonry; seismic assessment; structural interaction; experimental survey

1. Introduction

The vulnerability assessment of existing masonry buildings is a heavily investigated research topic due to the number of earthquakes that strike the southern area of Europe, as well as other countries throughout the world, causing the loss of lives and extensive damage to building stocks. Existing ancient masonry buildings, which are an important part of the identity of a country, appear to be particularly vulnerable. After the shocks, in situ survey campaigns have allowed identifying the principal characteristic collapse mechanisms of masonry buildings due to earthquake excitations [1–4]. Starting from the 1976 Friuli earthquake (Italy), Non-Linear Analysis approaches began to be used to assess the seismic capacity of masonry structures [5,6]. In the following years, the pushover analyses were proposed in the literature (see, e.g., [7–9]). They rapidly became the reference method to evaluate existing buildings, as prescribed in several Codes [10–13] and are nowadays generally applied by practitioners. In more recent years, Non-Linear Dynamic Analyses have been used in research studies, and also in the professional field, as a proper alternative tool, especially in the case of more complex buildings. The capacity of the structure is evaluated by the application of a suitable number of earthquake records, natural or artificially generated, and is compatible with the local spectrum [14]. The analyses are

run on Finite Element Models or on Discrete Element Models. The former ones describe the capacity of buildings with "box behaviour" well, and the latter ones can also seize the out-of-plane rocking and the out-of-plane collapse of masonry piers [15–19]. In any case, the computational costs are high, but isolated standalone buildings, monuments or churches of historical relevance can be analysed.

In historic towns, buildings are aggregated and joined together; their current appearance often deriving from subsequent interventions and additions that have occurred at different times and with different masonry textures or construction materials. Demolitions and reconstructions of some parts may have taken place, making it difficult nowadays to understand the effectiveness of the mutual constraints. The task is open, and recent research has begun to address it [20–22].

Dynamic ambient tests can be a valuable aid in calibrating FEM models to be used for the analyses [23], and they can also bring different behaviours of the various parts of complex buildings or blocks of houses to the forefront [24]. Similar techniques are employed in dynamic damage detection methods for structural health purposes [25–27].

In the present paper, the seismic assessment of a case study of a 175-year-old building complex in Udine (Italy) provides an opportunity to use the results of ambient dynamic tests together with the results of the study of the historic documentation, traditional in situ tests, and numerical analyses to understand the structural behaviour of the complex.

The building, called "Padiglione Lodi", was built in 1847 as a charity home for destitute people and extended and renovated several times afterwards. The structure is made of masonry, with limited use of concrete at the beginning of the 20th century. It consists of a main building and three wings (western, central and eastern). The inspections, experimental survey and analysis of the available documentation are used to calibrate a Finite Element Model of the whole complex. Moreover, they allow to single out the central wing as the unit needing more careful investigation. Ambient dynamic testing is then applied to the central wing in order to further validate the model and improve the knowledge of the interaction of the unit with the rest of the building.

Ambient dynamic tests turn out to be a useful and reliable procedure to understand the mutual interference of the different aggregate units and thus approach the analysis of an interconnected building complex.

2. Case Study: The XIX Century "Padiglione Lodi" Building Complex

A top view of the "Padiglione Lodi" building complex is shown in Figure 1.
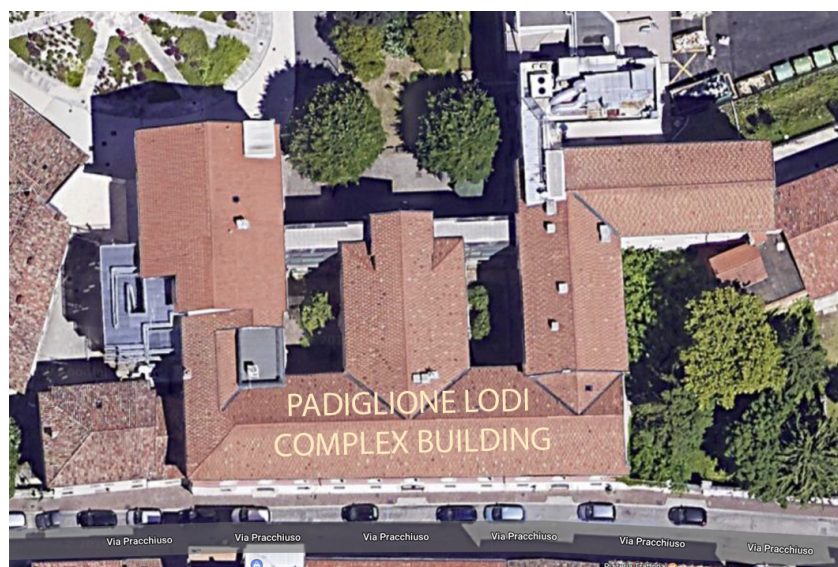

Figure 1. Top view of the "Padiglione Lodi" building complex.

Construction of the building began in 1847. It is currently used as a retirement home. It was also used as a military hospital several times in the past. As can be seen from Figure 2, the complex is currently composed of a main building and three wings, eastern, central and western. The main building has three floors above ground and is 12 m tall. The eastern and western wings are 14 m tall and also have three floors above ground. The central wing has two floors and hosts a church on the top floor. Lastly a block consisting of footbridges at each floor, indicated in pale yellow in Figure 2, connects the eastern, central and western wings.
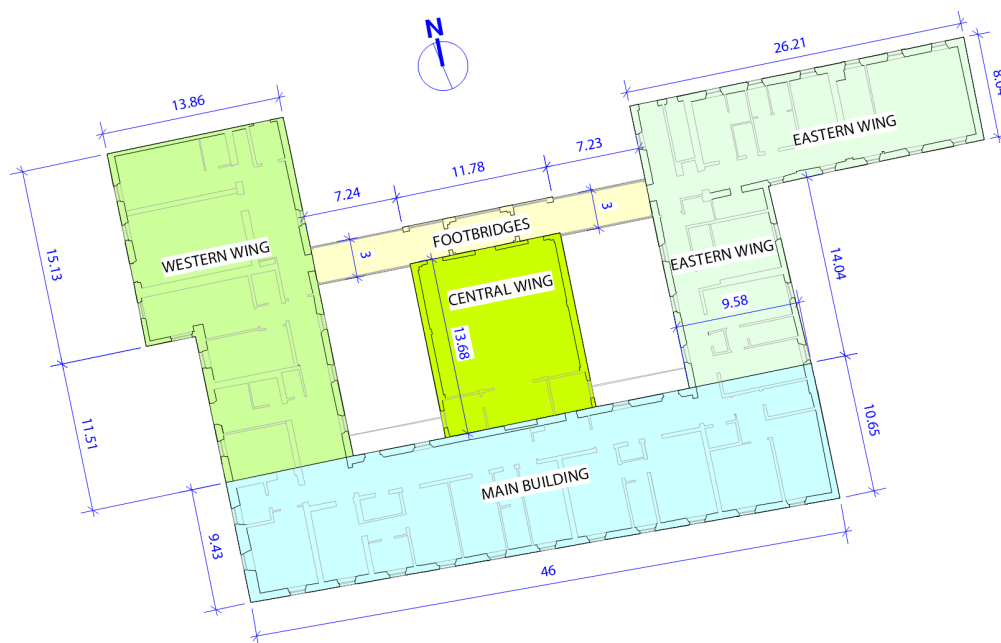

Figure 2. Plan of the "Padiglione Lodi" building complex.

Little is known about the history of interventions the building has undergone in the past. There is, however, a quite complete documentation regarding the most recent renovation works, which took place in 2001–2005. It entails a description of the previous state of the building, calculation reports, and architectural and structural drawings with construction details. The renovations affected mainly the eastern and western wings.

Despite some limited demolitions and reconstructions (especially in the west wing) and some strengthening measures such as the addition of reinforced concrete walls against existing walls in specific points during the 2001–2005 intervention, the main load bearing elements are still represented by brick or stone walls. This is especially the case for the main building. On a side but remarkable note, the columns sustaining the church on the first floor of the central wing are made of unreinforced concrete. The covering structure is in timber. With the exception of the wooden floor of the church in the central wing, all the floors are in hollow brick and concrete topping.

3. In Situ Experimental Survey

The objective of the in situ experimental survey is to achieve knowledge of the materials and of the load bearing structure of the building of level 2 according to the Italian Construction Code. This means that the in situ checks on the structural elements and their mutual connections are "exhaustive and extensive", while the tests on material properties are sufficiently extended.

To begin with, the geometry of the building complex was acquired by means of a detailed topographic survey and through the architectural and structural drawings of the 2001–2005 renovations.

As far as the unreinforced masonry walls are concerned, visual inspections through the removal of the lime plaster coating were carried out in twelve points, often chosen at the intersection between walls, in order to check their mutual connection as well. In each case, the area of the masonry surface brought to light amounted to about one square meter. Furthermore, in all of the twelve locations, penetrometer tests were performed on mortar to estimate an indicative value of the compressive strength [28]. The results are reported in Table 1. The average value of estimated compressive strength is 7.7 MPa, which corresponds to a mortar of class M5 according to the Italian Construction Code [29].

Table 1. Penetrometer tests on mortar.

#	Floor	Side	Masonry Type	Estimated Compressive Strength (MPa)
1	ground	external	crushed stone	6.2
2	ground	external	crushed stone	8.3
3	ground	external	solid bricks	4.2
4	ground	internal	crushed stone	10.0
5	ground	internal	solid bricks	5.2
6	first	internal	solid bricks	7.9
7	first	external	solid bricks	6.8
8	first	external	solid bricks	7.2
9	first	internal	solid bricks	17.1
10	second	internal	crushed stone	3.1
11	second	internal	solid bricks	6.4
12	garret	internal	solid bricks	10.3

Endoscopic tests were used in eight of the twelve locations to acquire data on the wall properties through depth. Two examples of the obtained results, one for a stone wall and one for a brick wall, are shown in Figure 3. Interestingly, of all inspected locations, no two presented identical compositions through the thickness.
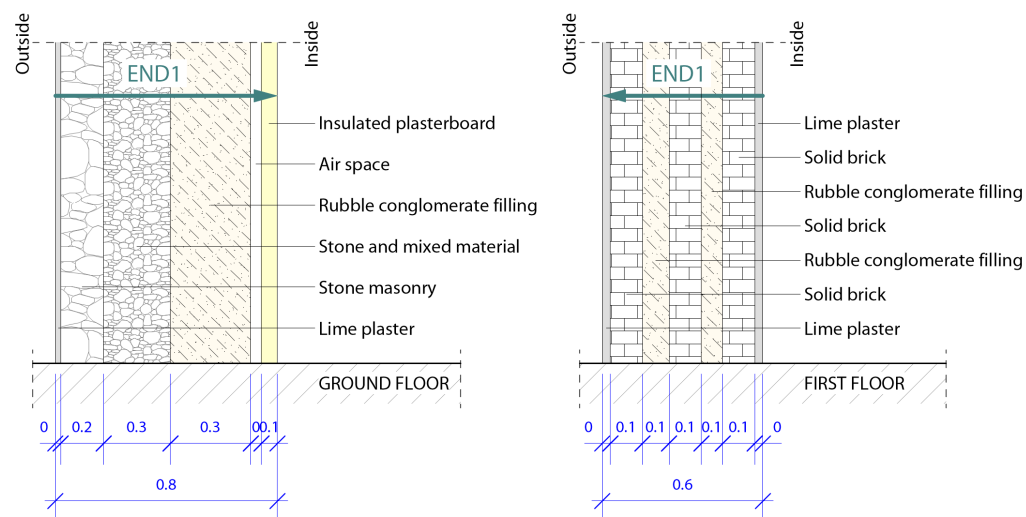

Figure 3. Example of wall characterisation through depth by means of endoscopic tests: stone wall (**left**) and brick wall (**right**).

Finally, in two positions on the ground floor, single and double flat jack tests were used, respectively, to assess the stress state and the mechanical properties of the masonry.

A picture of a double flat jack test appears in Figure 4a, while a picture of a single flat jack test is displayed in Figure 4b. The results are given in Table 2.

With respect to concrete and reinforced concrete elements, inspections and tests were integrated with the documentation of the 2001–2005 renovations and were located only in the wings of the building complex. Inspections were performed on seven horizontal

elements (beams, slabs) and one vertical element (a column of the central wing). Inspections included micro demolitions of the concrete cover and exposition of the rebars. A cover meter was also used as a non-destructive alternative. A limited number of material characterisation tests were also carried out. Two smooth steel reinforcement samples were extracted and subjected to tensile tests. Two concrete pull-out tests were executed in situ. Finally, four sonic rebound tests were used to locally estimate the concrete strength.
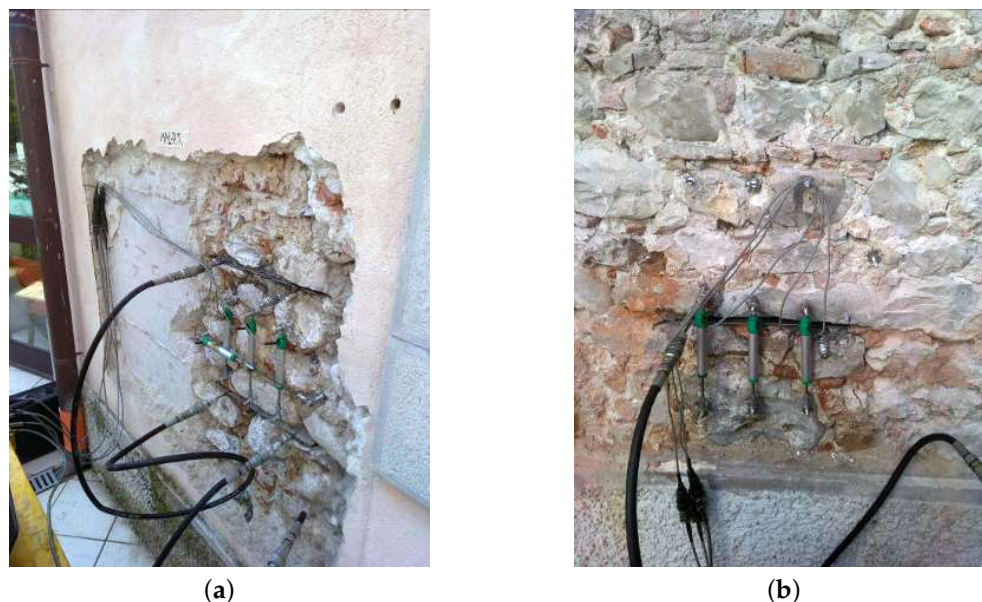

(a)   (b)

Figure 4. Flat jack tests. Location numbers according to Table 2. (**a**) Double flat jack test at location # 1. (**b**) Single flat jack test at location # 2.

Table 2. Flat jack test results.

| # | Floor | Location | Single Jack Compressive Stress (MPa) | Yield Stress (MPa) | Double Jack | | Poisson's Coefficient |
					Failure Stress (MPa)	Young's Modulus (MPa)	
1	ground	perimeter	1.00	5.00	13.33	1118	0.27
2	ground	internal	1.70	8.40	26.70	2501	0.35

The wooden roof structure was visually inspected for signs of deterioration, defects or termite attack. Eight locations were selected for quantitative testing. In each one, a hygrometer was first used to measure relative humidity, and then a penetrometer was applied to obtain a correlation with wood strength [30,31]. Finally, through thickness and density variation signalling, possible unseeable flaws were acquired by means of a calibrated resistance drill. In addition to these tests, a single specimen of roof rafter was taken from the west wing and subjected to a three-point bending test up to failure.

Floors were inspected visually and through small removals of material in thirteen selected locations. In this way, the construction type was confirmed, the reinforcement at the intrados was checked and the inter-axis of the joists were measured. Endoscopic tests were also carried out in ten of the thirteen locations, allowing for an examination of the floor across its thickness. Two in situ loading tests were conducted: the first, reaching a maximum load of 3 kN/m^2, on a hollow brick and concrete topping floor of the eastern wing; the second, reaching a maximum load of 4 kN/m^2, on the timber floor of the church in the central wing. Both tests featured seven measurement points for the out of plane displacement at the intrados of the floor.

Finally, two excavations along the external perimeter of the building complex allowed the measurement of the depth of the extrados and intrados of the footing.

4. Dynamic Testing on the Central Wing

The study of the documentation of the 2001–2005 renovation works, the outcomes of the inspections, and the material testing all point to the central wing as the weakest spot that deserves further investigation. This is due mainly to the fact that on the ground floor of the central wing, the only load resisting elements are the unreinforced concrete columns supporting the church on the first floor. The external masonry walls of the church are stiffer and stronger than the columns below and have been partly strengthened in 2001–2005 by the addition of injected tendons. Despite this, the masonry walls are also particularly slender given their two-floor height without an intermediate floor.

4.1. Description of the Experimental Campaign

Dynamic testing was used as an additional investigative tool for the central wing. Twelve accelerometers were employed. Eight sensors were placed in the central wing. Four sensors were placed on the main building in order to assess the independence of the vibration modes of the central wing. The position and direction of the measurement points on the first floor, second floor and garret are shown in Figure 5. Axes *X* (parallel to the longer side of the main building), *Y* (parallel to the shorter side of the main building) and *Z* (elevation) are also shown in Figure 5.
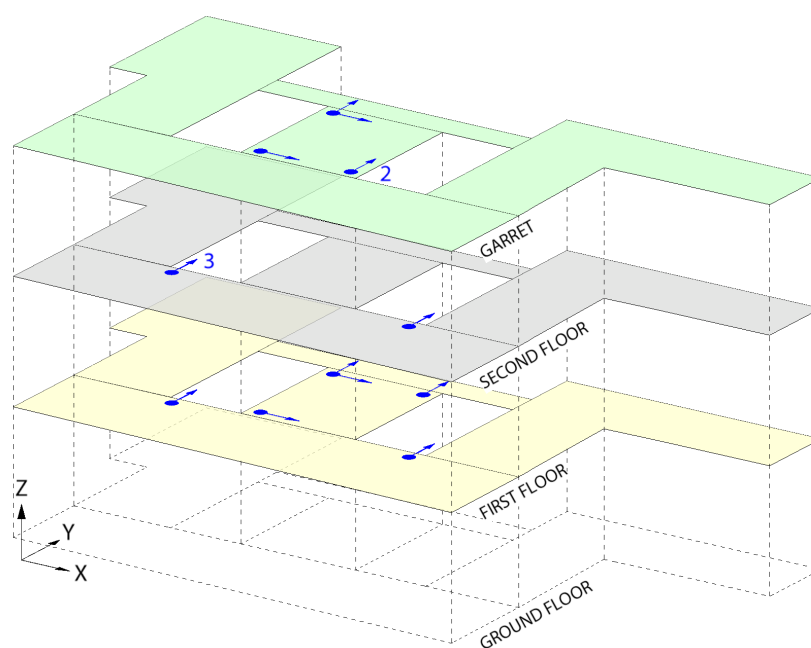

Figure 5. Position and direction of the accelerometers.

The accelerometers employed have a sensitivity of 10 V/g, a frequency range 0.1–20,000 Hz and a resolution higher than 8 μg RMS. They are connected in series to a signal conditioner, an antialiasing filter with a cutoff frequency of 20 Hz, and finally, to the dynamic multi-channel acquisition system.

4.2. Data Elaboration and Modal Analysis Results

From the recorded time histories, the power spectral density functions were calculated. The power spectral density matrix was obtained as the average of the power spectral density of all recordings. The extraction of modal parameters from the frequency domain responses was performed by means of the "PolyMAX Modal Parameter Estimation Method" [32,33]. The method allows estimating the modal parameters through the minimisation of a suitable error function once the order has been chosen (and therefore the number of poles) in which the power spectral density matrix can be decomposed. Basically, the modal identification process proceeds starting from models having a much higher order than the number of

modes actually present. Spurious modes fictitiously introduced are then excluded from the physical ones resorting to the stabilisation diagram.

The analysis of the ambient vibration response has led to the identification of the main modal vibration frequencies. A summary of the results is shown in Table 3.

Table 3. Experimental vibration frequencies of the central wing extracted from the 0–15 Hz frequency interval. Comparison with the numerically obtained frequencies is included.

Mode	Frequency (Hz)			Description
	Experimental	Numerical	% Error	
1X	5.82	5.36	−7.8	Translation in direction X
1Y	6.90	7.09	+2.7	Translation in direction Y
1T	7.42	7.17	−3.3	Torsional mode around axis Z. Weakly coupled with translation in dir. Y.

The vibration modes with dominant displacement components, e.g., in direction X (Y), will be henceforth referred simply as "translational mode X (Y)". A representation of the modes is given in Figures 6–8.
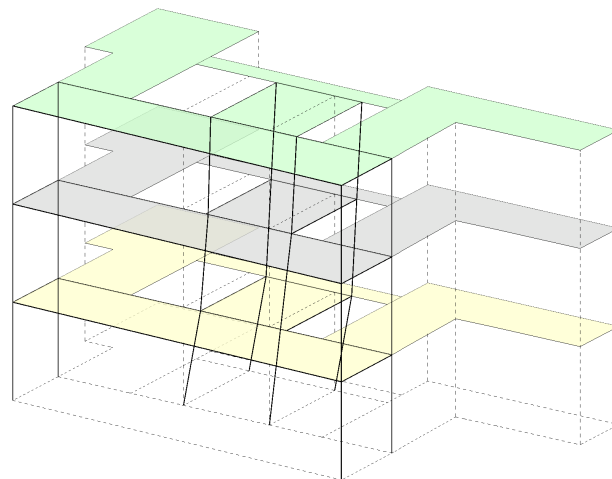

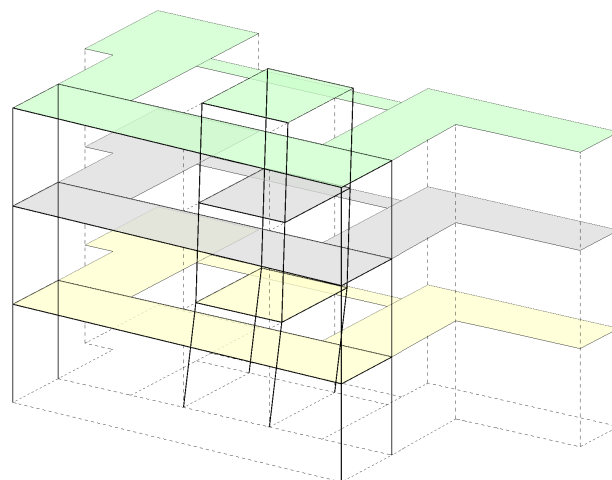**Figure 6.** Translational mode in direction X.

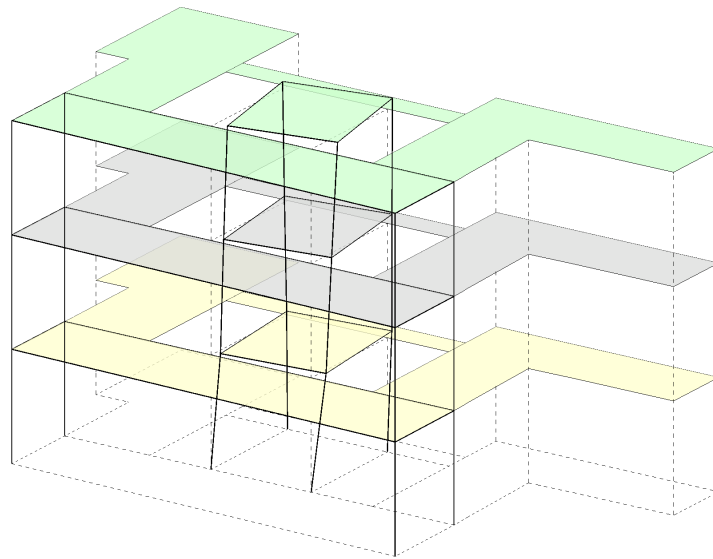**Figure 7.** Translational mode in direction Y.

Figure 8. Torsional mode around axis Z. Weakly coupled with Y translation.

Translation and rotation of the floors are computed under the assumption of in-plane rigid floors. The first three vibration modes correspond, respectively, to translational modes 1X, 1Y and to the fundamental torsional mode 1T. The first two modes are not coupled to rotations around axis Z. Mode 1T, instead, presents a certain degree of coupling between translation in direction Y and in-plane rotations. This can be justified by taking into account the closeness of the frequencies of modes 1Y and 1T, separated only by a 0.52 Hz difference. Table 3 also displays a comparison between experimentally and numerically obtained frequencies for the first three modes. The percentage error is below $\pm 10\%$ for all three modes. The finite element model used for the modal analysis is shown in Figure 9. The floors are assumed to be rigid in their plane. For an accurate explanation of the extracted experimental frequencies, it has been necessary to explicitly include the contribution to the stiffness of the exterior and interior curtain walls in the model, as shown in sand colour in Figure 9. Additional numerical validations performed by inserting a degree of connection between the main building and the central wing have also corroborated the independence of the central wing with respect to the main building.
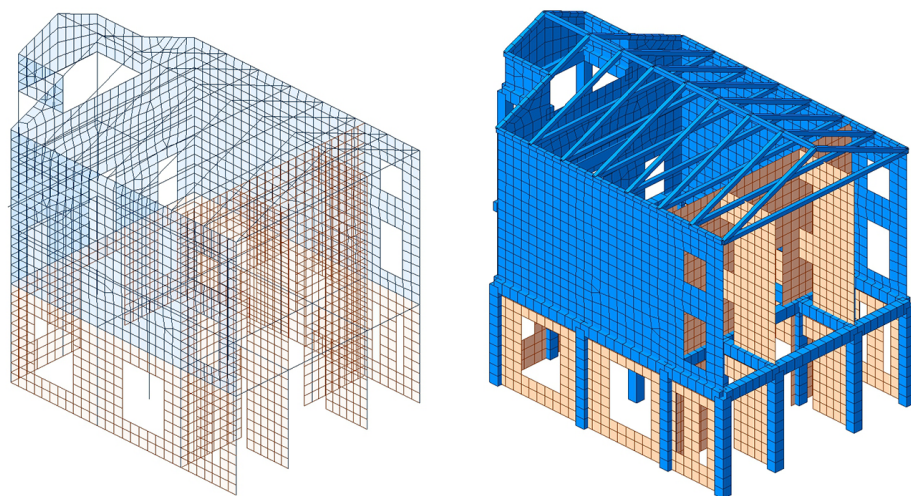

Figure 9. Wireframe (**left**) and solid (**right**) representation of the finite element model used for the modal analysis of the central wing.

The examination of the power spectral densities of the accelerometers positioned on the main building shows that the vibration amplitudes are negligible. An example is shown

in Figure 10, where the magnitude of the auto spectral density functions of two transducers recording accelerations in direction Y (see Figure 5 for reference) are compared: namely, accelerometer 2 positioned at the garret of the central wing and accelerometer 3 positioned at the second floor of the main building. The spectral density functions are not regular due to the very weak ambient excitation. The weakness of the excitation can also be inferred from the low magnitude of the maxima of the spectral density functions. In any case, the maximum magnitude of the auto spectral density function of accelerometer 2 placed on the central wing is about 3.5 times the maximum magnitude of accelerometer 3 placed on the main building.
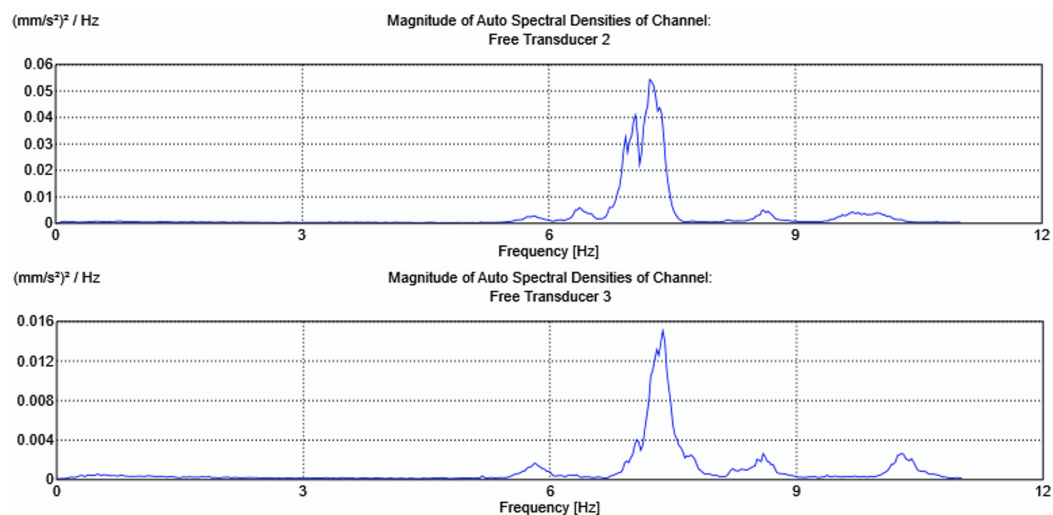

Figure 10. Magnitude of auto spectral density for accelerometer 2 (central wing, garret) and 3 (main building, second floor).

The central wing is, therefore, deduced to be independent with respect to the main building. This property allows performing separate seismic analyses and safety checks for structurally independent portions of the building complex.

4.3. Orthogonality Checks on the Experimental Vibration Modes

As well-known from structural dynamics, modal shapes satisfy a weighted orthogonality condition with respect to the mass distribution of the system. More precisely, denoting the mass matrix with $\mathbf{M}$ and with $\mathbf{U}^{(r)}$ the r-th mode of the vibrating system, one has

$$\mathbf{M}\mathbf{U}^{(r)} \cdot \mathbf{U}^{(s)} = \delta_{rs} \, , \tag{1}$$

where the Kronecker delta symbol δ_{rs} is equal to 1 if $r = s$ and 0 otherwise. Condition (1) is satisfied exactly when the vibrational modes include all the degrees of freedom of the system, and the mass matrix is correctly evaluated. Real situations are usually quite different because the degrees of freedom monitored represent only a fraction, often very small, of all the degrees of freedom in a discrete model of the structure. Moreover, errors in the estimate of the inertial properties of the system can increase the deviation from the ideal condition of in-plane rigid floors. Moreover, it may also occur that some experimental vibration modes correspond to modes that the analytical model used to compute the mass matrix is unable to describe. Table 4 shows the results of the orthonormality check on the experimental vibration modes. There are significant deviations from the ideal condition for the entries involving modes 1T and 1Y, for whom a certain degree of coupling had already been observed. For the other cases, the orthogonality requirement is acceptably met.

Table 4. Orthonormality checks on the first three experimental vibration modes. Percentage values.

Mode	1X	1Y	1T
1X	100	22	17
1Y	22	100	35
1T	17	35	100

5. Structural Vulnerability Assessment

The sequence of finite element models analysed for the structural vulnerability assessment of the "Padiglione Lodi" building complex is presented here. In the analyses, a reference earthquake with a return period of 712 years is used for the life safety limit state, and an earthquake with a return period of 75 years is used for the damage limitation limit states. These figures are based on the fact that retirement homes are assimilated into hospitals, according to national and local laws.

Methodologically, a static, linear elastic analysis of the whole complex is performed first. Then, exploiting the insight gained through dynamic testing and the detailed inspection and experimental survey, a separate non-linear static analysis is performed on the central wing alone. Although without the corroboration of dynamic testing, a similar separate analysis is then performed on the main building, which is the one to have been least renovated in recent years.

5.1. Material Parameters

The material parameters are identified based on the experimental survey of Section 3. The parameters for masonry are taken from ([34], Chapter 8.5). Their values are provided in Table 5. The strength design values used in the finite element model are obtained by dividing the values in Table 5 by the confidence factor equal to 1.2 and by the partial safety factor γ_M assigned according to the type of analysis performed.

Table 5. Adopted parameters for different masonry types.

Parameter	Hewn Blocks	Full Bricks	Hollow Bricks
Mean compression strength (MPa)	2.80	4.50	6.50
Mean shear strength (MPa)	0.06	0.12	0.13
Young's modulus (MPa)	1230	1500	5000
Shear modulus (MPa)	410	500	2000
Specific weight (kN/m^3)	20.0	18.0	15.00

Parameters for the other materials are also drawn from the Italian Building Code [29,34], once the average values have been estimated from the in situ experiments. These average values are in line with class C20/25 for concrete, and class C27 for the timber elements. FeB 44K is adopted for reinforcement steel. Early 20th century smooth, mild steel reinforcement is assigned type Aq 50 (see [35]).

5.2. Elastic Analysis of the Whole Structure

At first, a linear elastic static analysis of the whole structure is performed. The finite element model implemented in MIDAS [36] employs four node plate elements with 6 d.o.f at each node for the masonry walls and beam elements for reinforced concrete beams and columns and for the roof. An elastic foundation with a spring constant per unit surface equal to 40,000 kN/m^3 is adopted, corresponding to a refilled ground. The model, with 23,000 nodes, is shown in Figure 11.
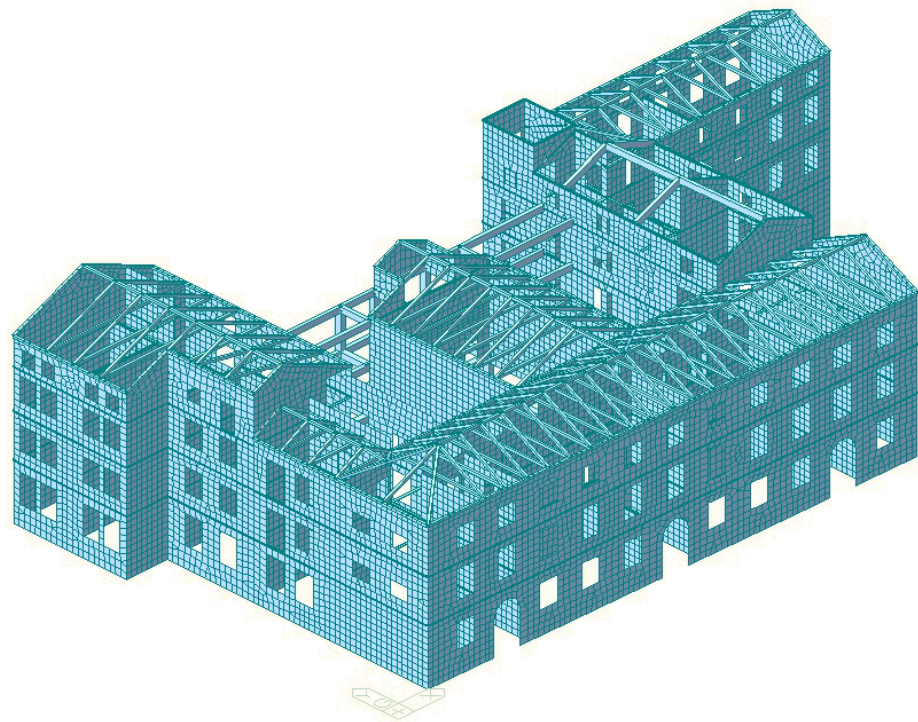
Figure 11. Finite element model used for the static, linear elastic analysis of the whole building complex.

The floors of each portion of the complex, i.e., the wings and the main building, are assumed rigid in their plane and not connected with each other. The results of the analysis under vertical loads at the ultimate limit states, as shown in Figure 12, highlight the most critical portions of the complex and guide subsequent, more detailed numerical investigations. The central wing, for example, noticeably presents local zones where the design strength of 1.2 MPa of the hewn stone walls is exceeded. Other similar local stress concentrations occur on the ground floor mainly in correspondence with wall openings with thin separations in between. However, this analysis does not account for material non-linearities, and in that setting, it is reasonable to expect a certain degree of redistribution. A satisfactory, albeit not quantified, level of safety against ultimate limit state vertical loads is to be expected for the building complex.
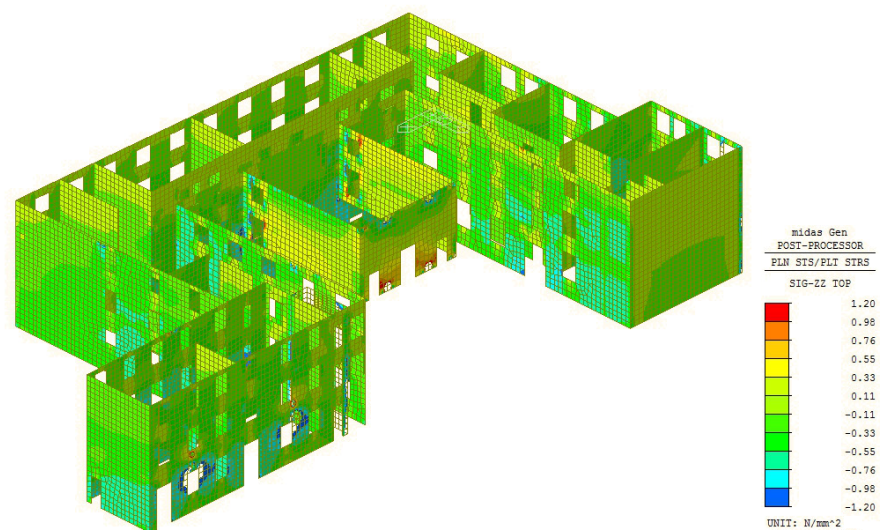

Figure 12. Linear static analysis at the ULS: vertical stress in the masonry.

5.3. Central Wing: Non-Linear Analysis and Seismic Verification

More in-depth, non-linear quasi static analyses are discussed next. Based on the experimental results of Section 4.2, the central wing is modelled as a separate entity. This modelling assumption is also substantiated by knowledge gathered during the building complex inspection relative to the loose mutual connection between the vertical walls and between the floors of the main building and of the central wing, respectively.

5.3.1. Model Description

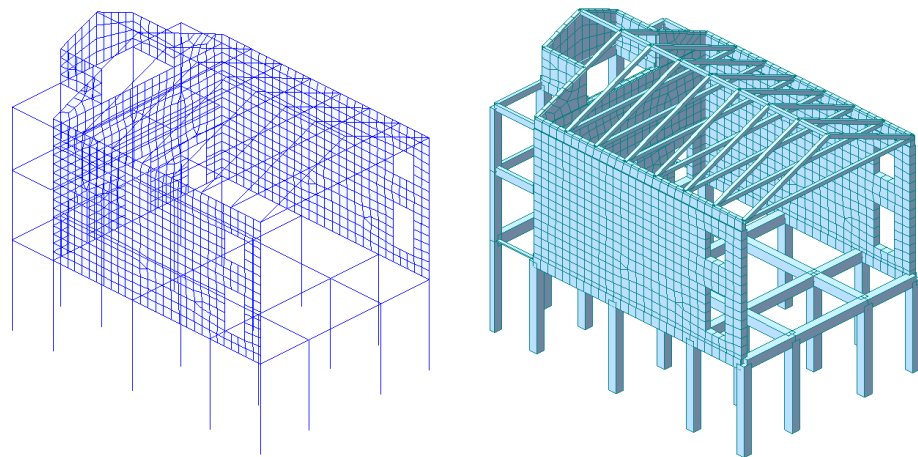A finite element model of the central wing is shown in Figure 13.

Figure 13. Wireframe (**left**) and solid (**right**) representation of the finite element model used for the non-linear analysis of the central wing.

As in the model of Section 5.2, beam elements are used for concrete columns and beams and for wooden roof beams; plate elements are used for masonry walls. At the ground floor, the only resisting elements are represented by the unreinforced concrete columns with a 0.5 by 0.5 m cross section. The masonry walls on the first floor, 0.27 to 0.38 m thick, are stronger and stiffer than the ground floor columns and exhibit a box-like behaviour.

Before performing the non-linear static analyses, an elastic analysis was carried out. As expected, the ground floor columns are confirmed to be the most stressed elements and are chosen as locations for plastic hinges. In a particular moment-rotation, plastic hinges are placed at the top cross sections of the columns. The constitutive behaviour is elastic–perfectly plastic with a brittle failure rotation threshold set at 1.5 times the limit elastic rotation. The limit moment for the unreinforced columns corresponds to the attainment of the 1.2 MPa design tensile strength. The limit moment has been computed for two different values of normal force, namely 200 and 400 kN, and is equal to 41.6 kN/m in the first case and to 58.3 kN/m in the second. Moreover, shear plastic connectors are placed at the mid points of the columns. Again, an elastic–perfectly plastic constitutive relationship is assumed. The failure displacement of the shear plastic connectors is set at 1.5 times the limit elastic one. The limit shear force of 77 kN is computed according to the Italian building code [29], neglecting the contribution of steel reinforcement.

A preliminary modal analysis is also carried out in order to determine the first translational mode in direction X (parallel to the longer side of the main building) and in direction Y (parallel to the shorter side of the main building). Both modes have an effective mass participation factor in their respective direction above 90%. Two non-linear static analyses are then performed, one with forces proportional to the first translational mode in direction X and one with forces proportional to the first translational mode in direction Y.

5.3.2. Results

Plots of the capacity (blue with red dots) and demand (green) curves in the rescaled spectral displacement vs. spectral acceleration coordinates are shown in Figure 14a,b for the seismic forces in direction X and Y, respectively. The bilinear capacity curve, obtained according to current building codes [29], is also shown in thin solid red.
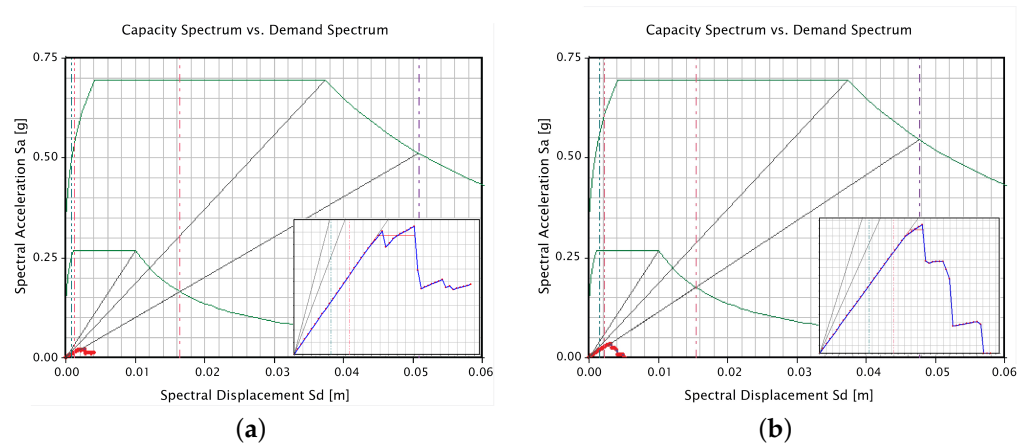

(a)　　　　　　　　　　　　　　　　　(b)

Figure 14. Seismic capacity and seismic demand curves for the SDOF equivalent system of the central wing. Displacements in the abscissae are in meters, and accelerations in the ordinates are in terms of gravitational acceleration, i.e., 1 corresponds to 9.8 m/s². The inset shows a zoom of the capacity curve. (**a**) Seismic forces in direction X. (**b**) Seismic forces in direction Y.

Results are summarised in Table 6. In both directions, the behaviour is extremely brittle and the demand much larger than the capacity: 20–24 times in the life safety limit state and 8–13 times in the damage limitation one.

Table 6. Seismic capacity and seismic demand displacements for the model of the central wing.

Direction of Seismic Forces	Damage Limitation Limit State			Life Safety Limit State		
	Demand (mm)	Capacity (mm)	d/c Ratio	Demand (mm)	Capacity (mm)	d/c Ratio
X	19.94	1.56	12.77	61.75	2.58	23.91
Y	14.67	2.16	6.80	45.45	2.29	19.85

5.4. Main Building: Non-Linear Analysis and Seismic Verification

Despite the lack of a specific experimental validation, a separate non-linear static analysis of the main building was also carried out. The choice is motivated by the same observations made during the inspection of the building complex and mentioned in Section 5.3, namely the loose connection between the vertical walls of the wings and the main building and the lack of continuity between the floors of the wings and the main building.

In this way, it is possible to carry out a more detailed non-linear analysis on a smaller portion of the complex and still gather relevant information.

5.4.1. Model Description

A wireframe and a solid view of the finite element model implemented in the software Midas Gen 2021 [36] is shown in Figure 15.
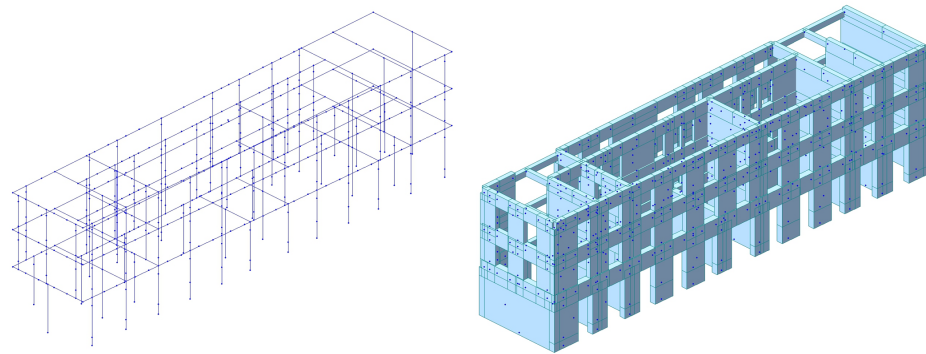
Figure 15. Wireframe (**left**) and solid (**right**) representation of the finite element model used for the non-linear analysis of the main building.

Masonry walls are modelled using beam elements by means of an equivalent frame method proposed by Dolce [37]. Moment-rotation plastic hinges are placed at the end nodes of masonry beam elements and shear force–displacement plastic connectors are placed at the mid point of the masonry elements. The constitutive law is elastic–perfectly plastic and is defined according to the prescriptions of the Italian building codes [34]. A diaphragm constraint is applied to the first and second floors and to the garret so that the seismic shear force is redistributed to the masonry walls according to their stiffness.

Two non-linear analyses are performed: one with a distribution of forces proportional to the first translational mode in direction X parallel to the longest side of the main building and one with a distribution of forces proportional to the first translational mode in direction Y parallel to the shortest side of the main building. Both modes have an effective mass participation factor of 77–78%.

5.4.2. Results

Plots of the capacity (blue with red dots) and demand (green) curves in the rescaled spectral displacement vs. spectral acceleration coordinates are shown in Figure 16a,b for the seismic forces in direction X and Y, respectively. The bilinear capacity curve, obtained according to current building codes [29], is also shown in thin solid red.
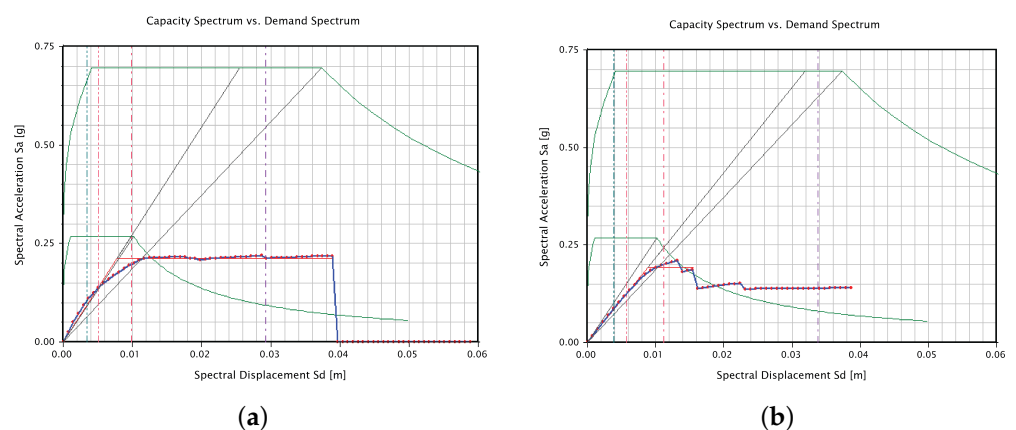

Figure 16. Seismic capacity and seismic demand curves for the SDOF equivalent system of the main building. Displacements in the abscissae are in meters, accelerations in the ordinates are in terms of gravitational acceleration, i.e., 1 corresponds to 9.8 m/s^2. (**a**) Seismic forces in direction X. (**b**) Seismic forces in direction Y.

Results are summarised in Table 7. The behaviour is ductile in the longitudinal direction X and brittle in the transverse direction Y. Seismic demand exceeds the seismic capacity for all limit states and force directions considered except for the life safety limit

state in direction X. However, the demand to capacity ratios are less severe by one order of magnitude than those of the central wing, with values ranging around 1–3 rather than 10–30.

Table 7. Seismic capacity and seismic demand displacements for the model of the main building.

Direction of Seismic Forces	Damage Limitation Limit State			Life Safety Limit State		
	Demand (mm)	Capacity (mm)	d/c Ratio	Demand (mm)	Capacity (mm)	d/c Ratio
X	13.26	7.60	1.75	39.49	39.86	0.99
Y	14.46	7.46	1.94	43.77	15.12	2.89

6. Conclusions

The conservation of the historical heritage, often consisting of masonry buildings, in earthquake prone areas is a well-known challenge. The case study analysed herein regards a complex consisting of several interconnected building units. These complexes and, in particular, the mutual connection of their units are the subject of a relatively recent and still ongoing research interest. In addition to an extensive experimental survey, which has provided quantitative estimates of the properties of the materials, it has been here decided to employ dynamic ambient vibration testing as a tool able to provide information about mutual constraints between units. In this specific application, the results have provided evidence that has allowed the analysis of one wing of the complex separate from the others, thus significantly simplifying the modelling. The ensuing finite element analyses have shown that the seismic capacity of the central wing in particular is inadequate and that the weak point is represented by the unreinforced concrete columns on the first floor where brittle failures take place. Similar but less critical deficiencies have emerged as well from the numerical analyses of the main building. Of course, more analogous experiences are required to further test the application of dynamic testing in the context of masonry building complexes, but the results obtained here seem to point to a promising extension of this methodology.

References

1. Spence, R.; D'Ayala, D. Damage Assessment and Analysis of the 1997 Umbria-Marche Earthquakes. *Struct. Eng. Int.* **1999**, *9*, 229–233. [CrossRef]
2. D'Ayala, D.F.; Paganoni, S. Assessment and analysis of damage in L'Aquila historic city centre after 6th April 2009. *Bull. Earthq. Eng.* **2010**, *9*, 81–104. [CrossRef]
3. Lorenzoni, F.; Caldon, M.; da Porto, F.; Modena, C.; Aoki, T. Post-earthquake controls and damage detection through structural health monitoring: Applications in l'Aquila. *J. Civ. Struct. Health Monit.* **2018**, *8*, 217–236. [CrossRef]

4. Sorrentino, L.; Cattari, S.; da Porto, F.; Magenes, G.; Penna, A. Seismic behaviour of ordinary masonry buildings during the 2016 central Italy earthquakes. *Bull. Earthq. Eng.* **2018**, *17*, 5583–5607. [CrossRef]

5. Tomaževič, M. *Computation of the Shear Resistance of Masonry Buildings*; Technical Report; Institute for Testing and Research in Materials and Structures-ZRMK: Ljubljana, Slovenia, 1978.

6. Tomaževič, M.; Turnšek, V. Lateral load distribution as a basis for the seismic resistance analysis of masonry buildings. In Proceedings of the International Research Conference on Earthquake Engineering, Skopje, Yugoslavia, 30 June–3 July 1980; pp. 455–488.

7. Fajfar, P.; Gašperšič, P. The N2 method for the seismic damage analysis of RC buildings. *Earthq. Eng. Struct. Dyn.* **1996**, *25*, 31–46. [CrossRef]

8. Krawinkler, H.; Seneviratna, G. Pros and cons of a pushover analysis of seismic performance evaluation. *Eng. Struct.* **1998**, *20*, 452–464. [CrossRef]

9. Elnashai, A.S. Advanced inelastic static (pushover) analysis for earthquake applications. *Struct. Eng. Mech.* **2001**, *12*, 51–69. [CrossRef]

10. Federal Emergency Management Agency (FEMA). *FEMA 440 Improvement of Nonlinear Static Seismic Analysis Procedures*; Federal Emergency Management Agency (FEMA): Washington, DC, USA, 2005.

11. CEN (European Committee for Standardization). *Eurocode 8: Design of Structures for Earthquake Resistance—Part 3: Assessment and Retrofitting of Buildings*; CEN (European Committee for Standardization): Brussels, Belgium, 2005.

12. Consiglio Nazionale delle Ricerche (CNR). *CNR-DT212 Recommendations for the Probabilistic Seismic Assessment of Existing Buildings*; Consiglio Nazionale delle Ricerche (CNR): Rome, Italy, 2013. (In Italian)

13. *ASCE/SEI 41-13 Seismic Evaluation and Retrofit of Existing Buildings*; American Society of Civil Engineers: Reston, VA, USA, 2014. [CrossRef]

14. Lagomarsino, S.; Cattari, S. Seismic Performance of Historical Masonry Structures Through Pushover and Nonlinear Dynamic Analyses. In *Perspectives on European Earthquake Engineering and Seismology: Volume 2*; Ansal, A., Ed.; Springer International Publishing: Cham, Switzerland, 2015; pp. 265–292. [CrossRef]

15. Baraldi, D.; Reccia, E.; Cecchi, A. In plane loaded masonry walls: DEM and FEM/DEM models. A critical review. *Meccanica* **2018**, *53*, 1613–1628. [CrossRef]

16. Gubana, A.; Melotto, M. Discrete-element analysis of floor influence on seismic response of masonry structures. *Proc. Inst. Civ. Eng.-Struct. Build.* **2021**, *174*, 459–472. [CrossRef]

17. Gubana, A.; Melotto, M. Evaluation of timber floor in-plane retrofitting interventions on the seismic response of masonry structures by DEM analysis: A case study. *Bull. Earthq. Eng.* **2021**, *19*, 6003–6026. [CrossRef]

18. Pantò, B.; Cannizzaro, F.; Caddemi, S.; Caliò, I. 3D macro-element modelling approach for seismic assessment of historical masonry churches. *Adv. Eng. Softw.* **2016**, *97*, 40–59. [CrossRef]

19. Chácara, C.; Cannizzaro, F.; Pantò, B.; Caliò, I.; Lourenço, P.B. Assessment of the dynamic response of unreinforced masonry structures using a macroelement modeling approach. *Earthq. Eng. Struct. Dyn.* **2018**, *47*, 2426–2446. [CrossRef]

20. Da Porto, F.; Munari, M.; Prota, A.; Modena, C. Analysis and repair of clustered buildings: Case study of a block in the historic city centre of L'Aquila (Central Italy). *Constr. Build. Mater.* **2013**, *38*, 1221–1237. [CrossRef]

21. Formisano, A.; Massimilla, A. A Novel Procedure for Simplified Nonlinear Numerical Modeling of Structural Units in Masonry Aggregates. *Int. J. Archit. Herit.* **2018**, *12*, 1162–1170. [CrossRef]

22. Degli Abbati, S.; D'Altri, A.M.; Ottonelli, D.; Castellazzi, G.; Cattari, S.; de Miranda, S.; Lagomarsino, S. Seismic assessment of interacting structural units in complex historic masonry constructions by nonlinear static analyses. *Comput. Struct.* **2019**, *213*, 51–71. [CrossRef]

23. Dilena, M.; Dell'Oste, M.F.; Gubana, A.; Morassi, A.; Polentarutti, F.; Puntel, E. Structural survey of old reinforced concrete elevated water tanks in an earthquake-prone area. *Eng. Struct.* **2021**, *234*, 111947. [CrossRef]

24. Morassi, A.; Polentarutti, F. Dynamic Testing and Structural Identification of the Hypo Bank Office Complex. II: Identification. *J. Struct. Eng.* **2011**, *137*, 1540–1552. [CrossRef]

25. Zhang, J.; Yi, T.H.; Qu, C.X.; Li, H.N. Detecting Hinge Joint Damage in Hollow Slab Bridges Using Mode Shapes Extracted from Vehicle Response. *J. Perform. Constr. Facil.* **2022**, *36*, 04021109. [CrossRef]

26. Zhang, J.; Yi, T.H.; Qu, C.X.; Li, H.N. Determining Orders of Modes Sensitive to Hinge Joint Damage in Assembled Hollow Slab Bridges. *J. Bridge Eng.* **2022**, *27*, 04022001. [CrossRef]

27. Caddemi, S.; Caliò, I.; Cannizzaro, F.; Morassi, A. A procedure for the identification of multiple cracks on beams and frames by static measurements. *Struct. Control Health Monit.* **2018**, *25*, e2194. [CrossRef]

28. Felicetti, R.; Gattesco, N. A penetration test to study the mechanical response of mortar in ancient masonry buildings. *Mater. Struct.* **1998**, *31*, 350–356. [CrossRef]

29. C. S. LL. PP. (Consiglio Superiore dei Lavori Pubblici). *Italian National Building Code "NTC 2018"*; Decree issued by the Italian Ministry of Infrastructure and Transportation: Rome, Italy, 17 January 2018. (In Italian)

30. Giuriani, E.; Gubana, A. A penetration test to evaluate wood decay and its application to the Loggia monument. *Mater. Struct.* **1993**, *26*, 8–14. [CrossRef]

31. Ronca, P.; Gubana, A. Mechanical characterisation of wooden structures by means of an in situ penetration test. *Constr. Build. Mater.* **1998**, *12*, 233–243. [CrossRef]

32. Guillaume, P.; Verboven, P.; Vanlanduit, S.; Van der Auweraer, H.; Peeters, B. A poly-reference implementation of the least-squares complex frequency-domain estimator. In Proceedings of the 21st IMAC Conference and Exposition 2003 (IMAC XXI), Kissimmee, FL, USA, 3–6 February 2003; Society for Experimental Mechanics (SEM): Bethel, CT, USA, 2003; pp. 1762–1770.
33. Peeters, B.; Van der Auweraer, H.; Guillaume, P.; Leuridan, J. The PolyMAX Frequency-Domain Method: A New Standard for Modal Parameter Estimation? *Shock Vib.* **2004**, *11*, 395–409. [CrossRef]
34. C. S. LL. PP. (Consiglio Superiore dei Lavori Pubblici). *Instructions for the Application of the Italian National Building Code "NTC 2018"*; Circular issued by the Italian Ministry of Infrastructure and Transportation on January 21st 2019; Published on the Gazzetta Ufficiale on February 11th 2019; 2019. Available online: www.gazzettaufficiale.it/eli/id/2019/02/11/19A00855/sg (accessed on 1 June 2022). (In Italian)
35. *Regio Decreto Legge Numero 2229, "Norme per L'esecuzione Delle Opere in Conglomerato Cementizio Semplice od Armato"*; National Building Code for Reinforced and Un-Reinforced Concrete. Now Obsolete; 1939. Available online: https://www.gazzettaufficiale. it/eli/gu/1940/04/18/92/so/92/sg/pdf (accessed on 1 June 2022). (In Italian)
36. *MIDAS Gen, Version 1.3*; Finite Element Software; MIDASIT Co. Ltd.: Seongnam, Korea, 2021.
37. Dolce, M. *Schematizzazione e Modellazione per Azioni nel Piano Delle Pareti*; Corso sul Consolidamento Degli Edifici in Muratura in Zona Sismica; Ordine Degli Ingegneri: Potenza, Italy, 1989.